Static Identification of Inductance Parameters and Initial Rotor Position in Permanent Magnet Synchronous Motor

Liyuan GUO, Chuanqiang LIAN, Guanda XU, Jilong LIU, Xin TANG, and Kun WANG

***Abstract*—Accurate determination of inductance parameters and rotor initial position is of paramount importance in ensuring optimal control accuracy and stability in the context of permanent magnet synchronous motors. This paper proposes a novel static identification method for both the inductance parameters and rotor initial position of a permanent magnet synchronous motor, to achieve simultaneous identification of both parameters. The method involves the injection of high-frequency quadrature voltage signals into the motor, followed by the decomposition of the high-frequency response current using the recursive least squares method. This results in the identification of the motor inductance parameters and rotor initial position, based on the outcomes of the motor rotor polarity identification. Compared with traditional methods, this approach has the advantages of eliminating the delay effect of digital system sampling and control, and of not requiring filters to demodulate the high-frequency response current. Furthermore, the identification results are less affected by the nonlinearity of the inverter. Both simulation and experimental validation support the validity of the method. The experimental results demonstrate that the errors between the identified values of the inductance of the cross and straight axes and the design value are 0.15% and 0.97%, respectively. Additionally, the deviation between the identified results and the actual value of the initial position of the rotor is 1.76°, indicating a high level of identification accuracy.**

***Index Terms*—High frequency injection; inductance parameter identification; initial position identification; permanent magnet synchronous motor.**

I. Introduction

THE permanent magnet synchronous machine (PMSM) is distinguished by its simple structure, high power density, high efficiency and low failure rate. It has found widespread application in a variety of fields, including aerospace, ships and vessels, and new energy vehicles.

The conventional identification methodologies for motor parameters can be categorised into two distinct approaches: offline identification methods, which include finite element analysis and experimental measurement [1], and online identification methods, encompassing recursive least squares [2]–[4], Kalman filter [5], [6] and artificial intelligence algorithms [7]. The offline identification method is characterized by its simplicity; however, it necessitates a substantial workload and often encounters challenges in achieving precise identification under full working conditions. Conversely, online identification can achieve identification under full working conditions, but the challenge of under-ranking remains. The inductance identification method based on finite element analysis considers the influence of the cross-saturation effect on the inductance of PMSM in the cross and straight axes. The obtained steady-state inductance parameters are essentially consistent with the actual measurement results, but the calculation process is more complicated. Another method identified in [1] involves the use of high-frequency square-wave voltage injection to identify the inductance parameters. This method takes into account the influence of inverter nonlinearity on the identification results. However, the delay caused by the digital system sampling is approximated by one carrier cycle. The inductor parameter identification method based on the recursive least squares method is mentioned in [2], and the computational amount of this method is smaller than that of the traditional least squares method. However, it is prone to the phenomenon of "data saturation". In order to address this problem, [3] mentions the combination of dynamic forgetting factor and recursive least squares method for inductor identification. Another inductor identification method is proposed in [8], which is based on double time scale stochastic approximation theory. This method is more accurate than the traditional recursive least squares algorithm. Additionally, an inductive parameter identification method based on Kalman filtering has been developed. This method utilizes the a posteriori probability density of the previous moment to iteratively obtain the a posteriori probability density of the subsequent moment. The results of this method are accurate; however, it is only applicable to linear systems. In addressing this limitation, subsequent scholars have proposed an extended Kalman filtering method for identifying motor inductance. This method involves the application of Kalman

Manuscript received January 01, 2025; revised March 02, 2025; accepted March 06, 2025. Date of publication June 30, 2025; date of current version April 18, 2025. This work was supported in part by China National Science Foundation under the Grant 52177202 and 52407230. *(Corresponding author: Chuanqiang Lian.)*

All authors are with National Key Laboratory of Electromagnetic Energy, Naval University of Engineering, Wuhan 430033, China (e-mail: glyisgreat@163.com; wzdslcq@163.com; 3150101258@zju.edu.cn; 66976@163.com; tangxin11@alumni.nudt.edu.cn; 28076622@qq.com).

Digital Object Identifier 10.24295/CPSSTPEA.2025.00012

filtering in nonlinear systems, as outlined in [7]. The proposed approach utilizes a chaotic initialization and a chaotic variation strategy to facilitate rapid identification of inductance parameters. However, the complexity of this method hinders its practical application in engineering contexts.

The conventional approach to rotor initial position identification can be categorized into two distinct methods: the dynamic identification method, which includes the rotor pre-positioning method [9], and the static identification method, which encompasses various high-frequency signal injection methods [10]−[16]. The high-frequency injection signals employed in these methods include high-frequency rotating voltage [10], high-frequency pulsating voltage [11], [12], high-frequency square-wave voltage [13]−[15], and triangular wave voltage [16]. The dynamic identification method is straightforward in principle, but it has certain requirements on the operating environment of the motor, and the identification results are easily affected by the rotation of the motor. Static identification can achieve high-precision identification, but the principle is more complex. [9] proposed a rotor initial pre-positioning method to identify the initial position, the essence of which is to inject a constant voltage vector into the motor for a certain period of time so that the motor rotor reaches a predetermined position. The method is simple but time-consuming and prone to phenomena such as reversal. A rotor initial position identification method based on high-frequency rotating voltage injection is introduced in [11]. The method involves the injection of a high-frequency rotating voltage into a stationary coordinate system, the extraction of the phase difference of the positive-sequence current to compensate for the phase of the negative-sequence current, and the final determination of the initial position of the rotor through the inverse tangent operation. This method has been demonstrated to exhibit high measurement accuracy; however, it necessitates the implementation of a low-pass filter to facilitate the demodulation of the response current. Moreover, it does not consider the impact of sampling and control delays that are inherent to digital systems. In contrast, [12] introduces a rotor initial position identification method based on high-frequency pulsed vibration injection. This method involves injecting a high-frequency pulsed vibration voltage into the estimated *d*-axis, demodulating the estimated *d*-axis currents and *q*-axis currents, and then locking the phase, thereby obtaining the initial position of the rotor. This method eliminates the need for a low-pass filter to demodulate the response current; however, it does not account for the effects of sampling and control delays in digital systems. [15] expounds on a rotor initial position recognition method that is predicated on high-frequency square wave injection. The fundamental principle underlying this method entails the injection of a high-frequency square wave signal into the estimated *d*-axis, followed by the acquisition of the initial rotor position through the analysis and processing of the estimated *q*-axis current response. The method exhibits reduced phase delay and enhanced detection accuracy; however, it is susceptible to inverter nonlinearity and switching loss, and its robustness is inadequate.

In light of the challenges posed by the conventional high-frequency injection technique, this paper puts forward a static identification method for the parameters of permanent magnet synchronous motor inductance and the initial rotor position. The proposed method involves the injection of high-frequency quadrature voltage signals into permanent magnet synchronous motor, utilising the recursive least-squares method. The method involves decomposing the high-frequency response currents of the motor orthogonally, thereby obtaining an estimation of the motor's inductance parameters and the initial position of its rotor. This process culminates in the identification of the rotor's polarity by leveraging the saturation characteristics of the inductance to rectify the estimated value. The saturation property of the inductor is then employed to identify the rotor polarity, and the estimated value of the rotor's initial position is corrected.The method's feasibility and effectiveness are verified by simulation and experimental results. In comparison with traditional methods, the proposed approach offers distinct advantages. It facilitates the simultaneous identification of inductor parameters and initial position, while also compensating for phase differences caused by sampling and control delays in the digital system during the identification process. This eliminates the necessity for approximate compensation with a fixed delay time, enhancing the accuracy of the parameter identification results. Furthermore, the method in this paper employs the recursive least squares method to demodulate the response current, obviating the necessity for a filter for demodulation. This approach effectively circumvents the signal delay and distortion problems that arise from the filter.

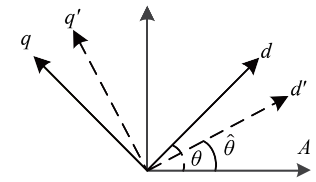

Fig. 1. Relationship between rotation coordinate system and estimated rotation coordinate system.

II. PMSM High Frequency Mathematical Modelling

The model of a three-phase permanent magnet synchronous motor at high frequency signals can be equated to a purely inductive model, as illustrated below:

$$\begin{cases} \dot{i}_{d\mathrm{h}} = \dfrac{1}{L_d} u_{d\mathrm{h}} \\ \dot{i}_{q\mathrm{h}} = \dfrac{1}{L_q} u_{q\mathrm{h}} \end{cases} \tag{1}$$

where, $u_{d\mathrm{h}}$、 $u_{q\mathrm{h}}$ is *d*, *q*-axis voltage; $i_{d\mathrm{h}}$、 $i_{q\mathrm{h}}$ is *d*, *q*-axis current; L_d、 L_q is *d*, *q*-axis inductance.

As illustrated in Fig. 1, the rotational coordinate system is shown to be related to the estimated rotational coordinate system. In this paper, the estimated rotational coordinate system is assumed to be in front of the A-phase winding axis θ , and the rotational coordinate system *d*-axis is shown to be ahead of the

A-phase winding axis $\hat{\theta}$. The size of $\hat{\theta}$ can vary, and to simplify the calculation, this paper sets $\hat{\theta}=0$. The angle difference between the rotational coordinate system and the estimated rotational coordinate system is $\Delta\theta=\theta-\hat{\theta}=\theta$, which is also the initial position of the motor rotor.

As illustrated in Fig. 1, the relationship between the motor voltage and current in the rotating coordinate system and the estimated motor voltage and current in the rotating coordinate system is

$$\begin{bmatrix} u_{d\mathrm{h}} \\ u_{q\mathrm{h}} \end{bmatrix} = \begin{bmatrix} \cos\Delta\theta & \sin\Delta\theta \\ -\sin\Delta\theta & \cos\Delta\theta \end{bmatrix} \begin{bmatrix} u'_{d\mathrm{h}} \\ u'_{q\mathrm{h}} \end{bmatrix}$$
$$\begin{bmatrix} i_{d\mathrm{h}} \\ i_{q\mathrm{h}} \end{bmatrix} = \begin{bmatrix} \cos\Delta\theta & \sin\Delta\theta \\ -\sin\Delta\theta & \cos\Delta\theta \end{bmatrix} \begin{bmatrix} i'_{d\mathrm{h}} \\ i'_{q\mathrm{h}} \end{bmatrix} \tag{2}$$

Combining (1) and (2), the voltage equation of the three-phase permanent magnet synchronous motor in the estimated rotational coordinate system can be expressed as:

$$\begin{bmatrix} i'_{d\mathrm{h}} \\ i'_{q\mathrm{h}} \end{bmatrix} = \begin{bmatrix} a_{11} & a_{12} \\ a_{21} & a_{22} \end{bmatrix} \begin{bmatrix} u'_{d\mathrm{h}} \\ u'_{q\mathrm{h}} \end{bmatrix} \tag{3}$$

In (3), $u'_{d\mathrm{h}}$、$u'_{q\mathrm{h}}$、$i'_{d\mathrm{h}}$、$i'_{q\mathrm{h}}$ represent the high-frequency voltage and high-frequency current, respectively, in the estimated rotating coordinate system. Let $m=(L_d+L_q)/L_dL_q$, $n=(L_d-L_q)/L_dL_q$, then

$$\begin{cases} a_{11} = \dfrac{m}{2} + \dfrac{n}{2}\cos(2\Delta\theta) \\ a_{12} = a_{21} = \dfrac{n}{2}\sin(2\Delta\theta) \\ a_{22} = \dfrac{m}{2} - \dfrac{n}{2}\cos(2\Delta\theta) \end{cases} \tag{4}$$

III. The Principle of Inductor Parameter and Initial Position Recognition in PMSM

As demonstrated in (4), the response current signal of the permanent magnet synchronous motor contains information regarding the inductance parameter and the initial position of the rotor. In this paper, an orthogonal decomposition of the high-frequency response current of the motor is employed, in conjunction with mathematical analysis, to ascertain the inductance parameter and the initial position of the rotor of the permanent magnet synchronous motor.

Firstly, it is necessary to set the angle between the estimated rotational coordinate system and the axis of the A-phase winding of the right-angle coordinate system to 0. Following this, a high-frequency quadrature voltage signal should be injected into the estimated rotational coordinate system of the permanent magnet synchronous motor. The given value of the high-frequency quadrature voltage at this time is

$$\begin{cases} u'_{d\mathrm{h}}{}^* = U_\mathrm{h}\cos(\omega_\mathrm{h} t) \\ u'_{q\mathrm{h}}{}^* = U_\mathrm{h}\sin(\omega_\mathrm{h} t) \end{cases} \tag{5}$$

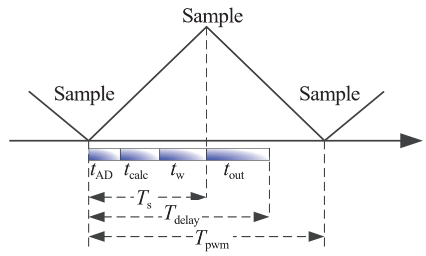

Fig. 2. PWM irregular sampling timing chart.

where, U_h is the high-frequency injection voltage amplitude and ω_h is the high-frequency injection voltage frequency.

In the context of an open-loop vector control system for a permanent magnet synchronous motor, it is evident that the digital system exhibits a delay phenomenon, resulting in a deviation between the actual and the desired voltage values. As illustrated in Fig. 2, the timing diagram of pulse width modulation (PWM) irregular sampling, the causes of the delay phenomenon include the signal A/D conversion time t_{AD} , the calculation time of the control algorithm t_{calc} , the waiting time to avoid the modulating signal and the carrier signal intercepted several times t_w , and the delay of the PWM output t_{out} . As the delay time of the digital system cannot be accurately measured, the conventional approach assumes that the delay time of the digital system is compensated by a fixed value. However, there is a discrepancy between this compensation value and the actual digital system delay time. This discrepancy generates a phase difference in the control system, thereby affecting the recognition accuracy of the motor parameters.

As demonstrated in Fig. 3, the time-domain waveforms of the injected voltage at varying frequencies are presented. The solid line waveform denotes the actual waveform, while the dashed line waveform indicates the given waveform. It is observed that as the frequency of the injected voltage increases, the phase difference between the actual and given waveforms also rises.

The method proposed in this paper is capable of cancelling the phase difference caused by the delay of the digital system in the identification process. This is due to the fact that the delay of the digital system is not a factor in this process. The high-frequency quadrature voltage signal after considering the digital system delay can be expressed as follows:

$$\begin{cases} u'_{d\mathrm{h}} = U_\mathrm{h}\cos(\omega_\mathrm{h} t + \varphi_\mathrm{e}) \\ u'_{q\mathrm{h}} = U_\mathrm{h}\sin(\omega_\mathrm{h} t + \varphi_\mathrm{e}) \end{cases} \tag{6}$$

where, φ_e is the phase difference of the injected quadrature voltage signal caused by the sampling and control delay of the digital system.

When combined with (3), the estimated high-frequency response current of the motor in the rotating coordinate system is expressed as follows:

$$\begin{cases} i'_{d\mathrm{h}} = \dfrac{U_\mathrm{h}}{\omega_\mathrm{h}}\left[A_{11}\sin(\omega_\mathrm{h} t) + A_{12}\cos(\omega_\mathrm{h} t)\right] \\ i'_{q\mathrm{h}} = \dfrac{U_\mathrm{h}}{\omega_\mathrm{h}}\left[A_{21}\sin(\omega_\mathrm{h} t) + A_{22}\cos(\omega_\mathrm{h} t)\right] \end{cases} \tag{7}$$

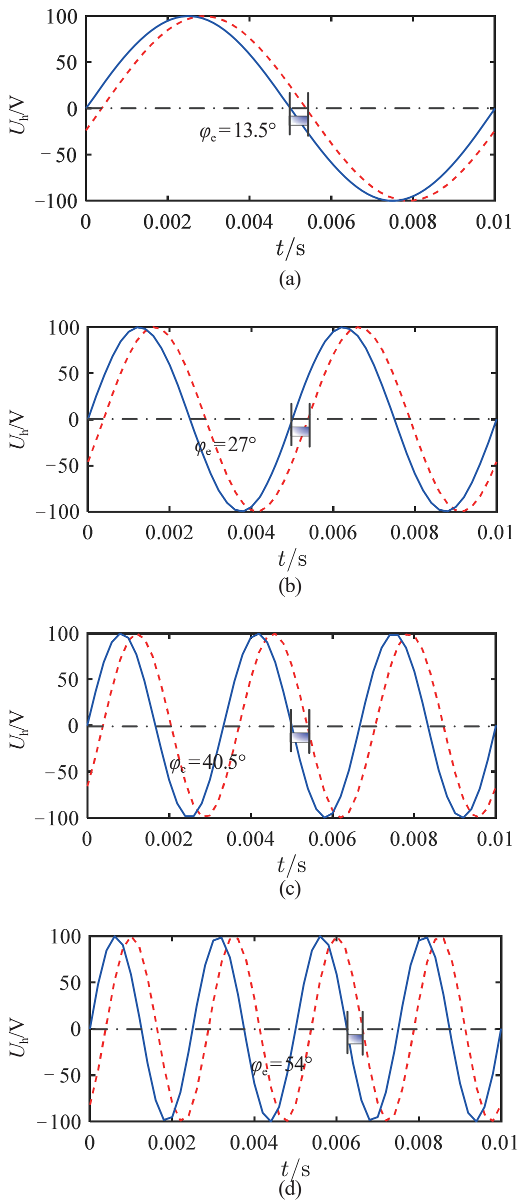

Fig. 3. Actual and given waveforms of injected voltage at different frequencies. (a) $|U_h|$ = 100 V, f_h = 100 Hz. (b) $|U_h|$ = 100 V, f_h = 200 Hz. (c) $|U_h|$ = 100 V, f_h = 300 Hz. (d) $|U_h|$ = 100 V, f_h = 400 Hz.

where,

$$\begin{cases} A_{11} = a_{11}\cos\varphi_e + a_{12}\sin\varphi_e \\ A_{12} = a_{11}\sin\varphi_e - a_{12}\cos\varphi_e \\ A_{21} = a_{21}\cos\varphi_e + a_{22}\sin\varphi_e \\ A_{22} = a_{21}\sin\varphi_e - a_{22}\cos\varphi_e \end{cases} \tag{8}$$

Meanwhile, (7) can be expressed as follows:

$$Y = \Phi^{\mathrm{T}} w \tag{9}$$

where,

$$Y = [\, i'_{dh} \quad i'_{qh} \,]^{\mathrm{T}} \tag{10}$$

$$\Phi^{\mathrm{T}} = \begin{bmatrix} \frac{U_h}{\omega_h}\sin(\omega_h t) & \frac{U_h}{\omega_h}\cos(\omega_h t) \\ \frac{U_h}{\omega_h}\sin(\omega_h t) & \frac{U_h}{\omega_h}\cos(\omega_h t) \end{bmatrix} \tag{11}$$

$$w = \begin{bmatrix} A_{11} & A_{21} \\ A_{12} & A_{22} \end{bmatrix} \tag{12}$$

The coefficients A_{11} , A_{12} , A_{21} and A_{22} contain the inductance parameter and the initial position information of the rotor. The present paper adopts the recursive least squares method to determine the size of the coefficients as follows:

$$\begin{cases} K(k) = P(k-1)\Phi(k)\left[\lambda I + \Phi^{\mathrm{T}}(k)P(k-1)\Phi(k)\right]^{-1} \\ P(k) = \frac{1}{\lambda}\left[I - K(k)\Phi^{\mathrm{T}}(k)\right]P(k-1) \\ e(k) = Y(k) - \Phi^{\mathrm{T}}(k)\,w(k-1) \\ w(k) = w(k-1) + K(k)e(k) \end{cases} \tag{13}$$

Following the determination of the coefficients A_{11} , A_{12} , A_{21} and A_{22} , which contain the motor inductance parameter and the rotor initial position parameter. The following assumption is made:

$$\begin{cases} y_1 = A_{11} - A_{22} = m\cos\varphi_e \\ y_2 = A_{12} + A_{21} = m\sin\varphi_e \\ y_3 = A_{11} + A_{22} = n\cos(2\Delta\theta - \varphi_e) \\ y_4 = A_{12} - A_{21} = -n\sin(2\Delta\theta - \varphi_e) \\ x_1 = \sqrt{y_1^2 + y_2^2} = m \\ x_2 = \sqrt{y_3^2 + y_4^2} = n \end{cases} \tag{14}$$

where,

$$\begin{cases} m = \frac{L_d + L_q}{L_d L_q} \\ n = \frac{L_d - L_q}{L_d L_q} \end{cases} \tag{15}$$

Performing mathematical analysis and derivation of (14), it can be demonstrated that the phase difference φ_e , caused by the digital system delay, can be eliminated. Consequently, the calculation formula for the motor inductance parameter and the initial position of the rotor can be obtained as follows:

$$\begin{cases} L_d = \frac{2}{x_1 + x_2} \\ L_q = \frac{2}{x_1 - x_2} \\ \Delta\theta = \frac{1}{2}\arctan\left(\frac{-y_4}{y_3}\right) + \frac{1}{2}\arctan\left(\frac{y_2}{y_1}\right) \end{cases} \tag{16}$$

In the absence of knowledge regarding the polarity of the motor rotor, the rotor initial position $\Delta\theta$, as specified in (16),

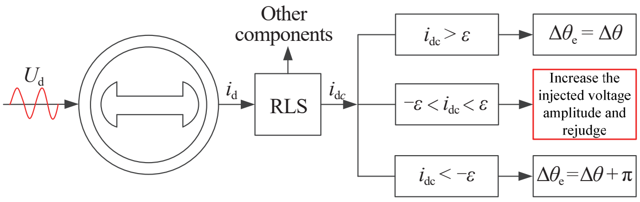

Fig. 4. Rotor polarity recognition strategy.

may correspond to the actual rotor initial position $\Delta\theta_e$, or may be in a direction antithetical to the actual rotor initial position $\Delta\theta_e$. Consequently, this paper aims to ascertain whether the rotor initial position necessitates compensation, contingent on an assessment of the motor rotor's polarity. The present paper introduces a method of detecting the average value of the DC component of the response current to verify the polarity of the rotor, as proposed in [17]. According to the saturation characteristics of the inductor, the magnitude of the DC component of the response current is determined to establish whether or not it is necessary to compensate for the initial rotor position. The specific polarity identification strategy is shown in Fig. 4.

In order to circumvent the impact of uncontrollable factors on the rotor polarity judgement in the context of actual engineering applications, this paper proposes a comparison parameter ε . When the response current DC component i_{dc} exceeds ε , the calculated rotor initial position aligns with the actual rotor initial position, obviating the necessity for compensation. Conversely, when the response current DC component i_{dc} falls short of $-\varepsilon$, the The calculated value of the rotor initial position is reversed with the actual position, and then the initial position is compensated by 180°. When the response current DC component i_{dc} is between $-\varepsilon$ and ε , the saturation characteristic of the motor magnetic circuit is not obvious, which is easy to cause the error of judging the rotor polarity. In this case, it is necessary to increase the amplitude of the injected voltage and judge the rotor polarity again.

As illustrated in Fig. 5, the method described in this paper is represented by a schematic flow diagram.

IV. Impact of Inverter Nonlinearity on Identification Results

A. Inverter Non-Linear Analysis

In a real motor drive system, the deadband of the inverter and the voltage drop of the switching devices have the capacity to distort the high frequency quadrature voltage signal that has been injected. This phenomenon is known as the inverter's non-linearity.

Subsequently, the high-frequency injection voltage of the permanent magnet synchronous motor, considering the inverter nonlinearity, can be expressed as:

$$\begin{cases} u'_{dh} = U_h \cos(\omega_h t + \varphi_e) + D_d V_{\text{dead}} \\ u'_{qh} = U_h \sin(\omega_h t + \varphi_e) + D_q V_{\text{dead}} \end{cases} \tag{17}$$

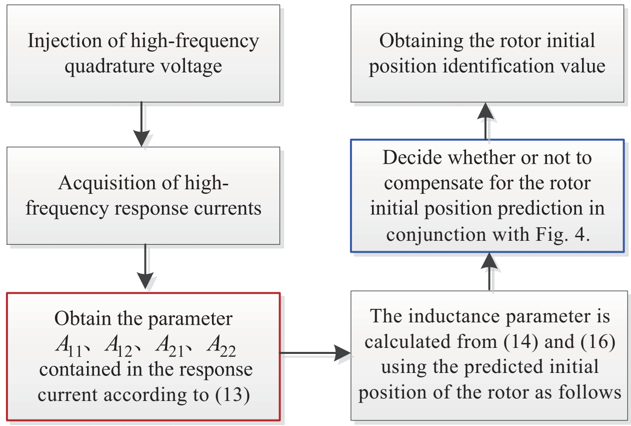

Fig. 5. Schematic flow diagram of the methodology of this paper.

where,

$$\begin{cases} D_d = \dfrac{4}{3}\cos\left(\mathrm{int}\left\{3(\theta_e + \gamma + \dfrac{\pi}{6})/\pi\right\}\dfrac{\pi}{3}\right) \\ D_q = \dfrac{4}{3}\sin\left(\mathrm{int}\left\{3(\theta_e + \gamma + \dfrac{\pi}{6})/\pi\right\}\dfrac{\pi}{3}\right) \end{cases} \tag{18}$$

$$V_{\text{dead}} = \frac{T_d + T_{\text{ON}} - T_{\text{OFF}}}{T_{\text{pwm}}}(V_{\text{dc}} - V_{\text{sat}} + V_f) + \frac{V_{\text{sat}} + V_f}{2} \tag{19}$$

In this system, the distortion coefficients of high-frequency quadrature voltage signal in the estimated rotating coordinate system are denoted by D_d and D_q . The electrical angle is indicated by θ_e , the current vector angle by γ , the dead time by T_d , the switching device turn-on and turn-off delays by T_{ON} and T_{OFF} , respectively, the switching period by T_{pwm} , the inverter DC voltage by V_{dc} , the voltage drop of the power supply switch by V_{sat} and the voltage drop of the switching device by V_f .

According to (17) and (18), the voltage deviation of the inverter due to its nonlinear characteristic is different when the rotor position is different. This change in voltage deviation will further change the amplitude of the high-frequency injected voltage, and the change in the amplitude of the high-frequency injected voltage will ultimately have an impact on the results of the identification of the inductor parameters with the initial position of the rotor. Fig. 6 provides a visual representation of the waveforms used to estimate the distortion coefficients in the rotating coordinate system. These waveforms are obtained by comparing the distortion coefficients with a given high-frequency injected voltage, which is used as a high-frequency fundamental noise reference.

B. Effect of Inverter Non-Linear on Parameter Identification Results

Combining (6) and (17) reveals that the voltage deviations caused by the inverter are $D_d V_{\text{dead}}$ and $D_q V_{\text{dead}}$. As illustrated in Fig. 6, this voltage deviation assumes the form of a square wave. According to the Fourier decomposition, the square wave can be expressed in the following:

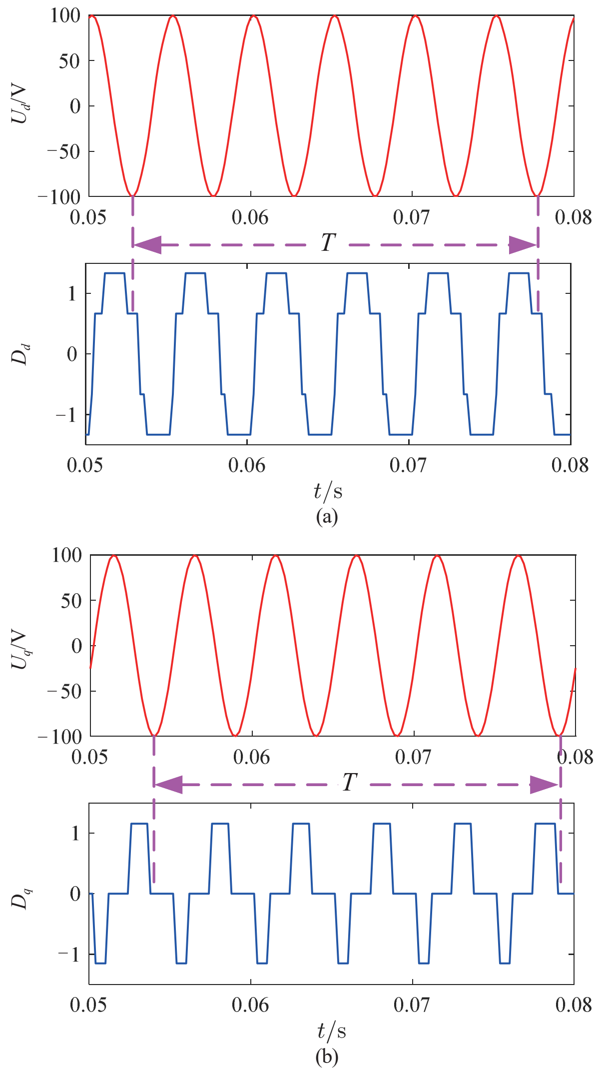

Fig. 6. Estimation of waveforms of distortion coefficients in a rotating coordinate system. (a) d-axis injection voltage and d-axis twist factor waveforms. (b) q-axis injection voltage and q-axis twist factor waveforms.

$$\begin{cases} D_d V_{\text{dead}} = a_0 + \sum_{n=1}^{\infty} a_n \sin(n\omega_h t) + \sum_{n=1}^{\infty} b_n \cos(n\omega_h t) \\ D_q V_{\text{dead}} = c_0 + \sum_{n=1}^{\infty} c_n \sin(n\omega_h t) + \sum_{n=1}^{\infty} d_n \cos(n\omega_h t) \end{cases} \tag{20}$$

As demonstrated in (7) to (16), the parameter identification process is confined to the high-frequency injected voltage sine and cosine fundamental components. That is to say, the parameters a_1, b_1, c_1 and d_1 in (20) have a significant impact on the outcomes of the parameter identification process. In order to obtain the values of a_1 , b_1 , c_1 and d_1 , a filter is first used to remove the high-frequency sine and cosine components of the voltage deviation. Then, the values of a_1 , b_1 , c_1 and d_1 are fitted using the recursive least squares method, and the fitting equations are as follows:

$$\begin{bmatrix} \Delta U_{d1} \\ \Delta U_{q1} \end{bmatrix} = \begin{bmatrix} 1 & \sin(\omega_h t) & \cos(\omega_h t) \\ 1 & \sin(\omega_h t) & \cos(\omega_h t) \end{bmatrix} \begin{bmatrix} a_0 & c_0 \\ a_1 & c_1 \\ b_1 & d_1 \end{bmatrix} \tag{21}$$

where, ΔU_{d1} and ΔU_{q1} are the voltage deviations with the high frequency sine and cosine components removed.

Subsequently, the high-frequency response current deviation resulting from this voltage deviation is as follows:

$$\begin{cases} \Delta i'_{dh} = \dfrac{U_h}{\omega_h}[\Delta A_{11}\sin(\omega_h t) + \Delta A_{12}\cos(\omega_h t)] \\ \Delta i'_{qh} = \dfrac{U_h}{\omega_h}[\Delta A_{21}\sin(\omega_h t) + \Delta A_{22}\cos(\omega_h t)] \end{cases} \tag{22}$$

where,

$$\begin{cases} \Delta A_{11} = (a_{11}b_1 + a_{12}d_1)/U_h \\ \Delta A_{12} = -(a_{11}a_1 + a_{12}c_1)/U_h \\ \Delta A_{21} = (a_{21}b_1 + a_{22}d_1)/U_h \\ \Delta A_{22} = -(a_{21}a_1 + a_{22}c_1)/U_h \end{cases} \tag{23}$$

The following equation is postulated:

$$\begin{cases} \Delta y_1 = \Delta A_{11} - \Delta A_{22} \\ \Delta y_2 = \Delta A_{12} + \Delta A_{21} \\ \Delta y_3 = \Delta A_{11} + \Delta A_{22} \\ \Delta y_4 = \Delta A_{12} - \Delta A_{21} \end{cases} \tag{24}$$

By combining (14), (16) and (24), the motor parameter identification equation that is independent of inverter nonlinearity can be introduced as follows:

$$\begin{cases} L'_d = \dfrac{2}{x'_1 + x'_2} \\ L'_q = \dfrac{2}{x'_1 - x'_2} \\ \Delta\theta' = \dfrac{1}{2}\arctan\left(\dfrac{-y_4 + \Delta y_4}{y_3 - \Delta y_3}\right) + \dfrac{1}{2}\arctan\left(\dfrac{y_2 - \Delta y_2}{y_1 - \Delta y_1}\right) \end{cases} \tag{25}$$

where,

$$\begin{cases} x'_1 = \sqrt{(y_1 - \Delta y_1)^2 + (y_2 - \Delta y_2)^2} \\ x'_2 = \sqrt{(y_3 - \Delta y_3)^2 + (y_4 - \Delta y_4)^2} \end{cases} \tag{26}$$

In this paper, (16) and (25) are utilised in the simulation to obtain the identification results of the motor parameters affected by the inverter nonlinearity and to remove the inverter nonlinearity, respectively. The deviations of these two equations are analysed under different dead times and different rotor positions. The d-axis inductance parameter is set to 3.1 mH and the q-axis inductance parameter is set to 6.8 mH, and the scalar values of the motor d-axis inductance parameter, q-axis inductance parameter and the rotor initial position deviation results are given in Figs. 7–9, respectively. As is apparent from Figs. 7–9, the identification error of the d-axis inductance parameter caused by the inverter nonlinearity is between 0.8% and 0.95%; the identification error of the q-axis inductance parameter is between 0.4% and 0.55%; and the identification error of the rotor initial position does not exceed 0.04°. The inverter nonlinearity

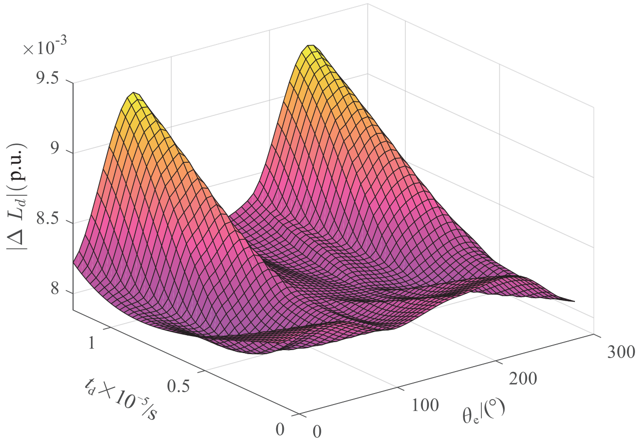

Fig. 7. *d*-axis inductor parameter identification deviation.

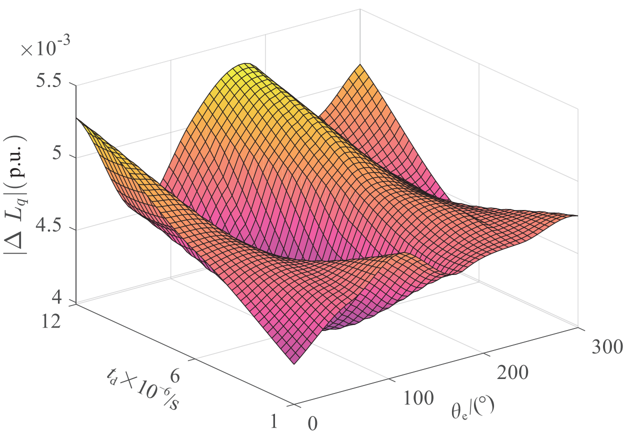

Fig. 8. *q*-axis inductance parameter identification deviation.

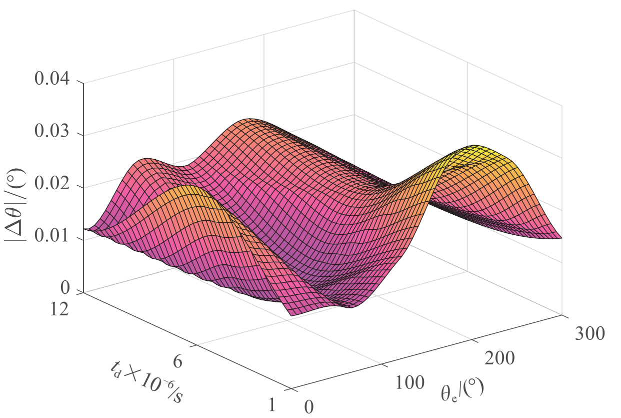

Fig. 9. Rotor initial position recognition deviation.

exerts a lesser influence on the motor parameter identification method proposed in this paper.

V. Simulation and Experimental Verification

A. Simulation Verification

In this paper, a proposed method of identifying the inductance parameter and rotor initial position of a permanent magnet synchronous motor is simulated and verified. The simulation model is constructed in MATLAB/Simulink according to the control block diagram in Fig. 10, and the relevant motor parameters during the simulation are presented in Table I.

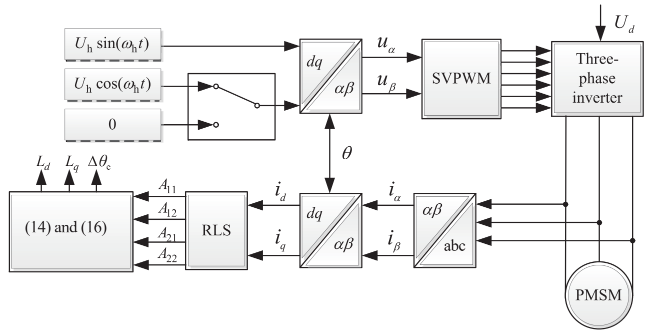

Fig. 10. Control strategy diagram.

TABLE I
Main Parameters of PMSM

Parameters	Value
Rated power	30 kW
Rated current	60 A
Stator resistance	0.05 Ω
Chain of permanent magnets	1.357 Wb
Moment of inertia (mechanics)	1 kg•m^2
d-axis inductance	3.1 mH
q-axis inductance	6.8 mH
Initial rotor position during simulation	0
Initial rotor position during experiment	180°
Sampling period	200×10^{-6} s
Polar logarithm	3

As illustrated in Fig. 11, the high-frequency injection voltage waveform and high-frequency response current waveform of the PMSM during simulation are shown, respectively. It is considered that the frequency of the high-frequency injection voltage should be set to 0.1−0.2 times the switching frequency. This is because if the frequency is set too high, it can easily generate other harmonic signals. However, if the frequency is set too low, it can easily separate from the fundamental signal. In this paper, the high-frequency injection voltage with an amplitude of 100 V and a frequency of 200 Hz is selected.

As illustrated in Fig. 12, the simulation results of the inductance parameters of the permanent magnet synchronous motor and the initial position of the rotor are presented. The parameter identification results converge within approximately 30 ms, with the identification results of the *d*-axis inductance and the *q*-axis inductance being 3.096 mH and 6.787 mH, respectively. The design value is only found in the error of 0.13% and 0.19%, respectively. It should be noted that the simulation of the motor model does not include saturation characteristics. Consequently, this paper does not include the simulation of motor rotor polarity

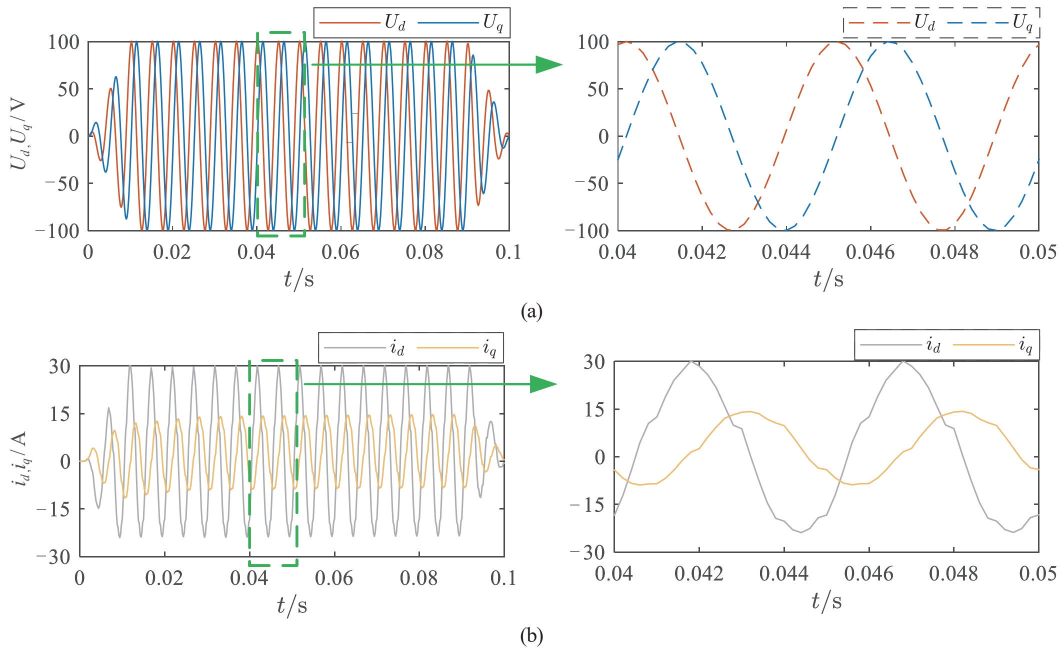

Fig. 11. High-frequency injection voltage and response current waveforms of PMSM during simulation. (a) High-frequency injection voltage waveform during simulation. (b) Response current waveform during simulation.

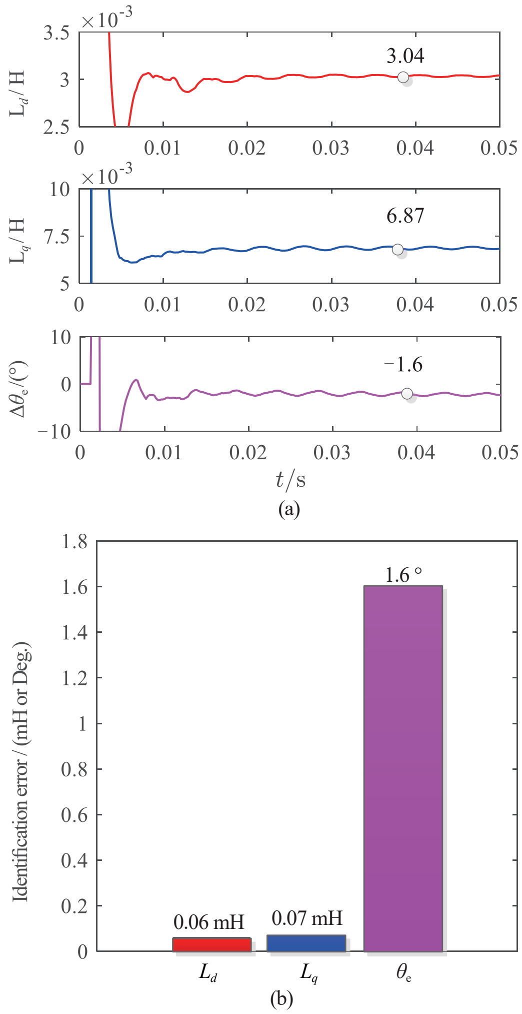

Fig. 12. Simulation identification results. (a) Simulation results. (b) Identification error.

identification, the default identification of the rotor initial position, and the actual rotor position in the same direction. However, in actual engineering applications, it is still necessary to carry out rotor polarity identification to determine the correctness of the rotor initial position identification results. This is demonstrated in 4.2 of the experimental demonstration. The identification results of the motor rotor initial position are −0.041°, and the simulation of the design value difference of 0.041°. The simulation results can better identify the motor parameters, and the identification results of the error are small.

Furthermore, the paper selects the motor parameters in Table I and applies the high-frequency pulse vibration injection method proposed in [12] and the high-frequency square wave injection method proposed in [15] to identify the motor parameters respectively. As the traditional high-frequency signal injection method is primarily used to identify the initial rotor position, this paper only focuses on the identification of the initial rotor position for comparative analysis. Fig. 13 illustrates the corresponding waveforms of the injected voltage and the identification results of the initial rotor position of the traditional method. As demonstrated in Fig. 13, the high-frequency pulsed voltage injection method requires approximately 70 milliseconds to complete the rotor initial position identification, yielding an identification error of 3.56°. In comparison, the high-frequency square-wave voltage injection method requires around 50 milliseconds to accomplish the same task, resulting in an identification error of 2.16°. A comparison of these two traditional methods with the method proposed in this paper clearly demonstrates the former's clear disadvantages in terms of rotor initial position identification, due to the fact that the proposed method is not only more accurate, but also faster.

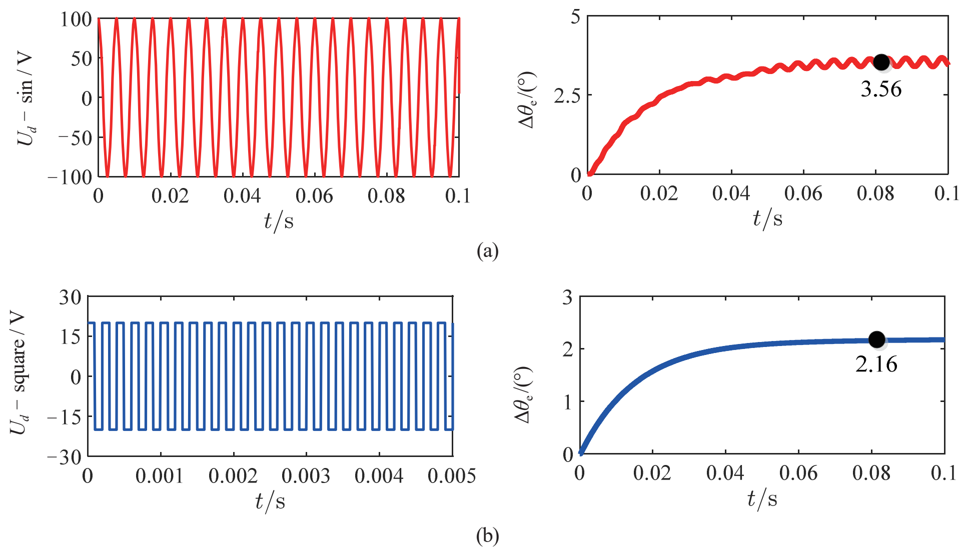

Fig. 13. Results of rotor initial position identification by conventional high-frequency injection method. (a) Localised map of PMSM rotor initial position identification results with injected signals based on high frequency pulsed vibration signal injection. (b) Localised map of PMSM rotor initial position identification results with injected signals based on high-frequency square-wave signal injection.

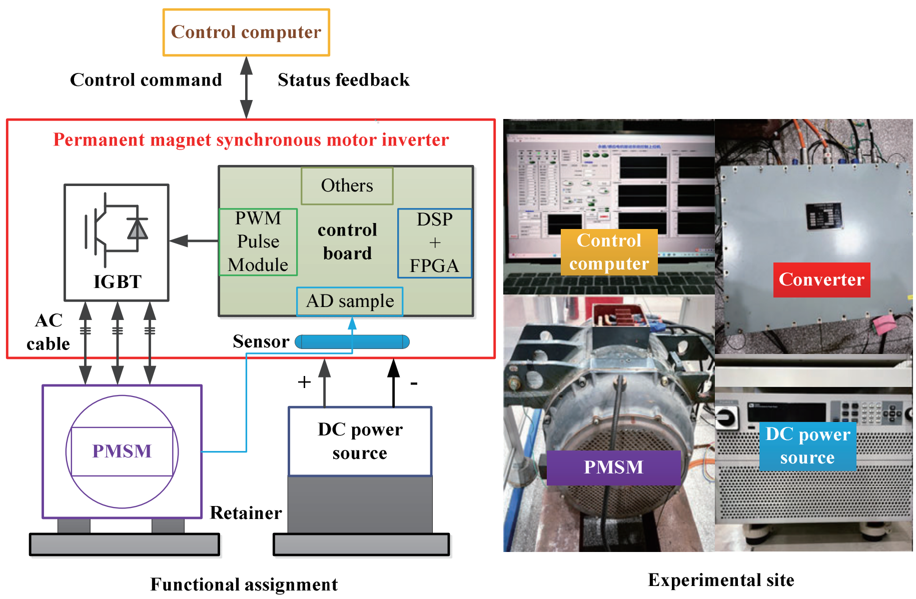

Fig. 14. Experimental platforms.

B. Experimental Verification

In this paper, the proposed method of identifying the inductance parameters and initial rotor position of permanent magnet synchronous motor is experimentally verified. The experimental platform is shown in Fig. 14, which mainly includes the power supply, inverter, permanent magnet synchronous motor and host computer, in which the inverter is a TMS320F28335 DSP and Cyclone IV FPGA as the core control chip. The parameters of the permanent magnet synchronous motor used in the experiment are shown in Table I. The DC side voltage is set to 500 V and the SVPWM switching frequency is 1 kHZ for the experiment.

In this experiment, $\hat{\theta}$ is assumed to be 0 at the moment 0, and a high-frequency quadrature voltage signal with an amplitude of 100 V and a frequency of 200 Hz is injected into the estimated rotating coordinate system of the PMSM. The computation of the inductance parameter and the estimated value of the rotor initial position is performed within the time frame of 0 to 0.1 s, while the rotor polarity identification and the correction of the estimated value of the rotor initial position is performed within the time frame of 0.1 to 0.16 s.

As illustrated in Fig. 15(a), the high-frequency injected voltage waveform of the PMSM during the experiment has been presented. In order to mitigate the impact effect on the motor when the quadrature voltage is injected, the amplitude change has been incorporated into the ramp function over a period of 0.01 s. Fig. 15(b) provides a representation of the high-frequency

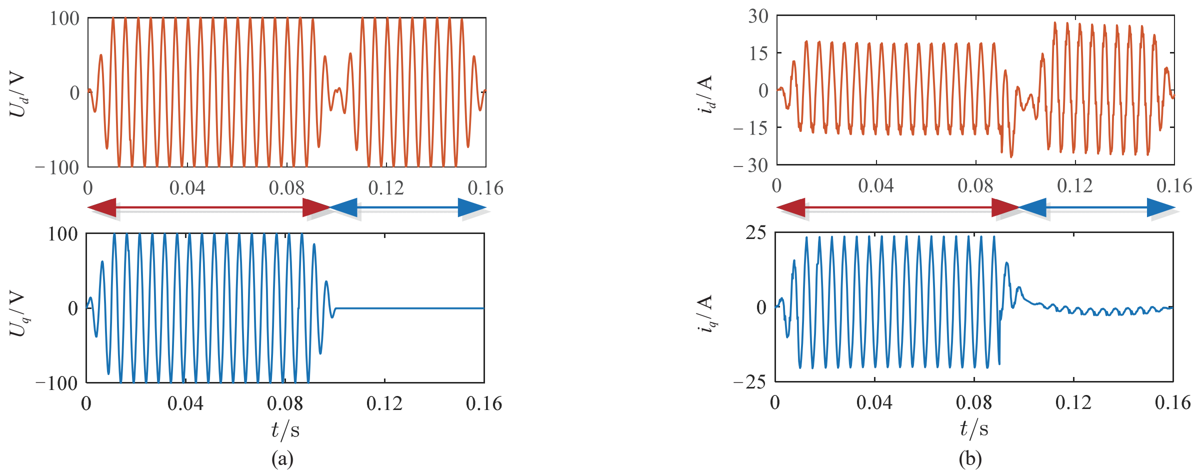

Fig. 15. High-frequency injection voltage and response current waveforms of PMSM during the experiment. (a) High frequency injection voltage wave form during experiment. (b) High frequency response current waveform during experiment.

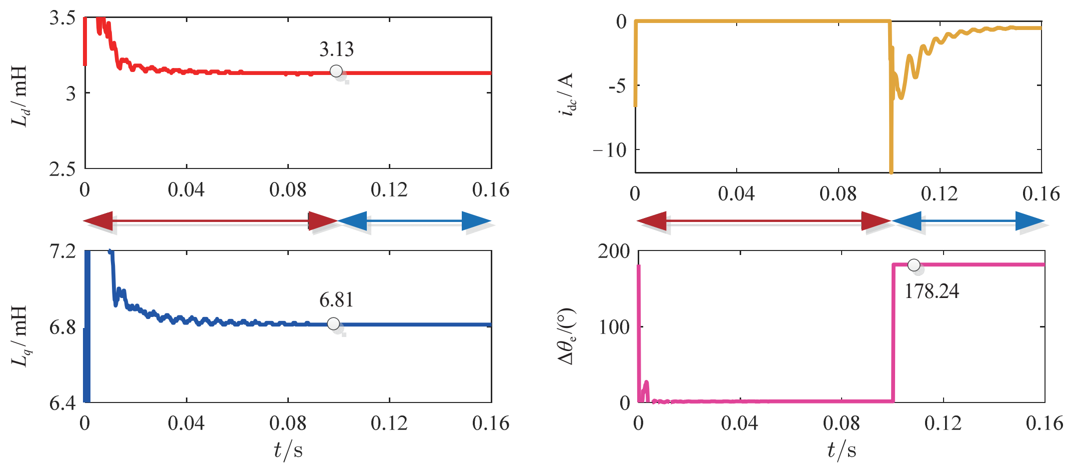

Fig. 16. Experimental identification results.

response current waveform of the PMSM.

As illustrated in Fig. 16, the results of identifying the DC component of the d-axis response current in the PMSM polarity identification stage are presented. The d-axis inductance, the q-axis inductance and the initial position of the rotor at the time of the experiment are used as the basis for these results. As demonstrated in the figure, the DC component is found to be negative. In accordance with the principle of polarity identification and compensation outlined in Fig. 4, it is evident that the calculated position of the rotor is opposite to its actual position at this time. The identification results of the d-axis inductance and the q-axis inductance have an error of 0.97% and 0.15%, respectively, compared with the design values of the PMSM in Table I. The initial rotor position of the motor used in the experiment is 180°, and the initial rotor position identified in this paper is 178.24°, which is close to each other. In summary, the identification results of this paper are accurate, and can complete the identification of inductance parameters in approximately 50 ms, and complete the identification of rotor initial position parameters in 160 ms.

In addition to the foregoing, a series of experiments were conducted in which the amplitude and frequency of the high-frequency injection voltage were varied. The inductance parameter specification obtained from these experiments is shown in Fig.17(a), while the deviation value of the rotor initial position recognition results is shown in Fig.17(b). It is evident from the data that, for a constant injection frequency, an increase in the amplitude of the selected injection voltage results in a reduction of the error between the identification results and the motor design values. Furthermore, it is evident that an enhancement in the high-frequency response current of the motor leads to a reduction in the parameter identification error and more accurate identification results.

VI. Conclusion

The control performance of permanent magnet synchronous motors (PMSM) is contingent upon the precise measurement of inductance parameters and the determination of the rotor's initial position. In this paper, a static identification method for the inductance parameters and rotor initial position of a permanent magnet synchronous motor is proposed. The proposed methodology involves the injection of high-frequency quadrature voltage signals into the motor, followed by the utilisation

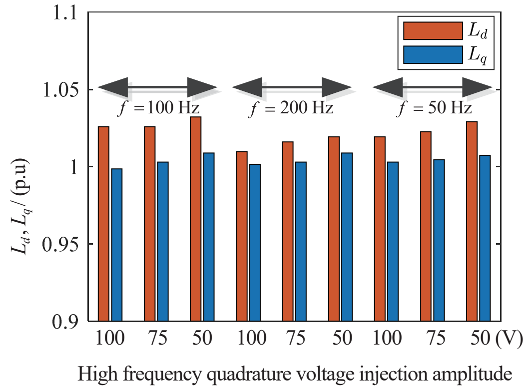

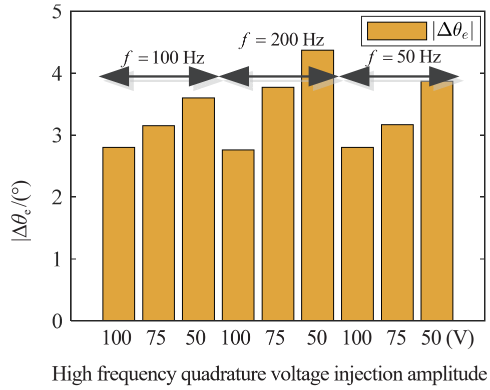

Fig. 17. Identification results for different injection voltages. (a) The process of inductive identification invariably results in the identification of the youngest valus. (b) The result of the identification of the initial position of the rotor exhibits a deviation value.

of the recursive least squares method for the decomposition of the high-frequency response currents of the motor. This process enables the estimation of the motor's inductance parameters and the initial rotor position. Subsequently, the estimated value of the initial rotor position is corrected in accordance with the saturation characteristics of the inductance. In comparison with the traditional method, the novel approach has the capacity to offset the phase difference caused by the sampling and control delay of the digital system. Furthermore, there is no necessity to utilise a filter for demodulation, which effectively avoids the signal delay and distortion caused by the filter. Additionally, it is less affected by the nonlinearity of the inverter.

In response to the research conducted in this paper, future endeavours will primarily encompass the reduction of the time required for the identification of the inductor parameters and the initial position of the rotor, as well as the compensation method for the inverter nonlinearity in the identification.

References

[1] K. Huang, J. Zhou, S. Liu, and S. Huang,"Inductance identification method of permanent magnet synchronous motor considering inverter nonlinearity based on high-frequency injection," in *Transactions of China Electrotechnical Society*, vol. 36, no. 8, pp. 1607–1616, 2021.

[2] J. Zhang, F. Peng, Y. Huang, Y. Hao, and Z. Zhu, "Online inductance identification using PWM current ripple for position sensorless drive of high-speed surface-mounted permanent magnet synchronous machines," in *IEEE Transactions on Industrial Electronics*, vol. 69, no. 12, pp. 12426–12436, Dec. 2022.

[3] Z. Ma, W. Zhang, J. He, and H. Jin, "Multi-parameter online identification of permanent magnet synchronous motor based on dynamic forgetting factor recursive least squares," in *Proceedings of 2022 IEEE 5th International Electrical and Energy Conference (CIEEC)*, 2022, pp. 4865–4870.

[4] C. Y. Jia, X. D. Wang, and K. Zhou, "Predictive control of built-in permanent magnet synchronous motor current model based on inductance identification," in *Journal of Electrical Machines and Control*, vol. 25, no. 11, pp. 75–82, 2021.

[5] Y. Zhang, Y. Bi, and S. Wang, "Parameter identification of permanent magnet synchronous motor based on extended Kalman filter and Gradient correction," in *Proceedings of 2020 IEEE International Conference on Mechatronics and Automation (ICMA)*, 2020, pp. 718–722.

[6] T. Hu, J. Liu, J. Cao, and L. Li, "On-line parameter identification of permanent magnet synchronous motor based on extended Kalman filter," in *Proceedings of 2022 25th International Conference on Electrical Machines and Systems (ICEMS)*, 2022, pp.1–6.

[7] H. Li and X. Jian, "Parameter identification of permanent magnet synchronous motor based on CGCRAO algorithm," in *IEEE Access*, vol. 11, pp. 124319–124330, 2023.

[8] C. Lian, F. Xiao, S. Gao, and J. Long, "Parameter identification for interior permanent magnet synchronous motor based on experimental calibration and stochastic approximation theory with two time scales," in *Proceedings of the CSEE*, vol. 39, no. 16, pp. 4892–4898, 4991, 2019.

[9] J. Liu, F. Xiao, Y. Shen, Z. Mai, and C. Li, "Position-sensorless control technology of permanent-magnet synchronous motor-a review," in *Transactions of China Electrotechnical Society*, vol. 32, no. 16, pp. 76–88, 2017.

[10] J. Yang, S. Yang, H. Li, and X. Zhang, "Initial rotor position estimation for IPMSM based on high frequency rotating voltage injection," in *Transactions of China Electrotechnical Society*, vol. 33, no. 15, pp. 3547–3555, 2018.

[11] A. Yu, L. Liu, Z. Kan, and C. Zhang, "Initial position identification of PMSM with filterless high frequency pulse signal injection method," in *Transactions of China Electrotechnical Society*, vol. 36, no. 4, pp. 801–809, 2021.

[12] Z. Mai, F. Xiao, K. Fu, J. Liu, C. Lian, K. Li, and W. Zhang, "HF pulsating carrier voltage injection method based on improved position error signal extraction strategy for PMSM position sensorless control," in *IEEE Transactions on Power Electronics*, vol. 36, no. 8, pp. 9348–9360, Aug. 2021.

[13] W. Li, J. Liu, and S. Chen, "Permanent magnet synchronous motor rotor position detection method based on high-frequency square-wave signal injection," in *Transactions of China Electrotechnical Society*, vol. 33, no. 24, pp. 5821–5829, 2018.

[14] C. Li, G. Wang, G. Zhang, N. Zhao, and D. Xu, "Adaptive pseudorandom high-frequency square-wave voltage injection based sensorless control for SynRM drives," in *IEEE Transactions on Power Electronics*, vol. 36, no. 3, pp. 3200–3210, Mar. 2021.

[15] K. Yu and Z. Wang, "Position sensorless control of IPMSM using adjustable frequency setting square-wave voltage injection," in *IEEE Transactions on Power Electronics*, vol. 37, no. 11, pp. 12973–12979, Nov. 2022.

[16] M. Sun, Y. He, X. Qiu, T. Tao, and W. Zhang, "Random frequency triangular wave injection based sensorless control of PMSM drives for audible noise reduction," in *Transactions of China Electrotechnical Society*, vol. 38, no. 6, pp. 1460–1471, 2023.

[17] B. Liu, "Research on rotor position detection technology of permanent magnet synchronous motor based on pulse high-frequency signal injection," Ph.D. dissertation, Dept. Elect. Eng., Nanjing University of Aeronautics and Astronautics, Nanjing, China, 2018.

Liyuan Guo was born in Shanxi, China, in 1999. He received the B.S. degree in electrical engineering from Shanxi University, Taiyuan, China, in 2022. He is currently working toward the M.S. degree with the National Key Laboratory of Electromagnetic Energy, Naval University of Engineering, Wuhan, China. His current research area is high-performance control of permanent magnet synchronous motors.

Chuanqiang Lian received the B.S. degree in automation from the Department of Automation, Tsinghua University, Beijing, China, in 2008, and the M.S. and Ph.D. degrees from the College of Mechatronic Engineering and Automation (CMA), National University of Defense Technology (NUDT), Changsha, China, in 2010 and 2016, respectively. He is currently an Associate Professor with the National Key Laboratory of Electromagnetic Energy, Naval University of Engineering, Wuhan, China. He has co-authored over twenty papers in international journals and conferences. His current research interests include AC motor control and flywheel energy storage.

Guanda Xu was born in Jiangxi, China, in 1998. He received the B.S. degree in electrical engineering from Zhejiang University, Hangzhou, China, in 2019, and the M.S. degree from the Naval University of Engineering, Wuhan, China, in 2021. He is currently working toward the Ph.D. degree with the National Key Laboratory of Electromagnetic Energy, Naval University of Engineering, Wuhan, China. His research interests include position and current sensorless control of AC motors and electric vehicle drives.

Jilong Liu was born in Hebei, China, in 1988. He received the B.S. and Ph.D. degrees in electrical engineering from the School of Electrical Engineering, Xi'an Jiaotong University, Xi'an, China, in 2010 and 2015, respectively. From 2015 to 2017, he was a Lecturer with the National Key Laboratory of Electromagnetic Energy, Naval University of Engineering, Wuhan, China, where he was promoted to an Associate Professor in 2017, and to a Full Professor in 2022. His current research interests include modular multilevel converter and AC motor control.

Tang Xin was born in Sichuan, China, in 1989. He received the B.S. degree in mechanical engineering from Jilin University, China, in 2011; the M.S. and Ph.D. degrees in mechatronics engineering from the National University of Defense Technology, China, in 2014 and 2018, respectively. He is currently a lecturer at the Naval University of Engineering, Wuhan, China. His research interests mainly include condition monitoring, fault diagnosis and related AI modeling methods of power electronic devices.

Kun Wang was born in 1985, holds a master's degree in electrical engineering. He is currently a lecturer at the Naval University of Engineering, Wuhan, China.